

# Simulating Structure Formation of the Local Universe

Steffen Heß\*, Francisco-Shu Kitaura† & Stefan Gottlöber

*Leibniz-Institut für Astrophysik Potsdam (AIP), An der Sternwarte 16, D-14482 Potsdam, Germany*

4 October 2018

## ABSTRACT

In this work we present cosmological  $N$ -body simulations of the Local Universe with initial conditions constrained by the Two-Micron Redshift Survey (2MRS) within a cubic volume of  $180 h^{-1}$  Mpc side-length centred at the Local Group.

We use a self-consistent Bayesian based approach to explore the joint parameter space of primordial density fluctuations and peculiar velocity fields, which are compatible with the 2MRS galaxy distribution after cosmic evolution. This method (the KIGEN-code) includes the novel ALPT (Augmented Lagrangian Perturbation Theory) structure formation model which combines second order LPT (2LPT) on large scales with the spherical collapse model on small scales. Furthermore we describe coherent flows with 2LPT and include a dispersion term to model fingers-of-god (fogs) arising from virialised structures. These implementations are crucial to avoid artificial parallel filamentary structures, which appear when using the structure formation model with the 2LPT approximation and the data with compressed fogs. We assume  $\Lambda$ CDM cosmology throughout our method.

The recovered initial Gaussian fields are used to perform a set of 25 constrained simulations. Statistically this ensemble of simulations is in agreement with a reference set of 25 simulations based on randomly seeded Gaussian fluctuations in terms of matter statistics, power-spectra and mass functions.

Considering the entire volume of  $(180 h^{-1} \text{ Mpc})^3$  we obtain correlation coefficients of about 98.3% for the cell-to-cell comparison between the simulated density fields and the galaxy density field in log-space with Gaussian smoothing scales of  $r_S = 3.5 h^{-1}$  Mpc (74% for  $r_S = 1.4 h^{-1}$  Mpc). The cross power-spectra show correlations with the galaxy distribution which weakens towards smaller length scales until they vanish at scales of  $2.2 - 3.0 h^{-1}$  Mpc.

The simulations we present provide a fully nonlinear density and velocity field with a high level of correlation with the observed galaxy distribution at scales of a few Mpc.

**Key words:** (cosmology:) large-scale structure of Universe – galaxies: clusters: general – catalogues – galaxies: statistics

## 1 INTRODUCTION

The leading paradigm in cosmology is given by hierarchical structure formation, in which the large-scale structure we observe today formed through gravitationally driven subsequent merging of objects of increasing size (see White & Rees 1978; Fry & Peebles 1978).

Cosmological simulations have played a major role in confirming this theory, obtaining structures statistically similar to the observed ones (see e. g. Davis et al. (1985); Springel et al. (2005) or for a recent review Kuhlen et al. (2012)). These studies use random seeded fluctuations per-

mitting one only to compare theoretical models to observations based on statistical properties (see e. g. the recent work studying the likelihood of large structures Park et al. 2012).

Such an approach relies on the cosmological principle implying that any sufficiently large observed region can be taken as a representative part of the Universe. Hence large surveyed volumes in which the Universe can be considered homogeneous are required to suppress the so-called “cosmic variance”. Large volume simulations are especially necessary to study the cosmic evolution of various signatures imprinted in the primordial density fluctuations, such as baryon acoustic oscillations (BAOs) (as in Kim et al. 2009; Prada et al. 2012; Angulo et al. 2012; Alimi et al. 2012). However, numerical  $N$ -body simulations become extremely expensive,

\* E-mail: shess@aip.de

† E-mail: kitaura@aip.de, Karl-Schwarzschild fellow

when in addition to large volumes the surveying of faint objects is required (i. e. high resolutions).

A complementary approach to the “cosmic variance” problem consists of trying to reproduce observed structures in the Local Universe. This would allow for a direct comparison between theory and observations. In this case smaller volumes are sufficient, since the particular cosmic realisation of the Universe is taken into account.

The concept of this approach is to reconstruct the initial density fields compatible with the galaxy distribution given a particular structure formation model. Cosmological  $N$ -body simulations using the phase information corresponding to these fields are expected to *naturally* reproduce the observed structures in the Local Universe. The quality of the phase information in the initial density fields determines the accuracy with which structures are reproduced by a cosmological  $N$ -body simulation. These kind of simulations are usually called “constrained simulations” (CS). Various methods have been used to obtain Gaussian fields given a set of constraints (see the seminal works by Bertschinger (1987); Hoffman & Ribak (1991); van de Weygaert & Bertschinger (1996) and the more recent ones Kitaura & Enßlin (2008); Kitaura et al. (2010); Jasche & Kitaura (2010); Kitaura et al. (2012)).

Hitherto, a number of pioneering attempts have followed this approach showing the large number of difficulties one encounters when trying to perform constrained simulations (see Kolatt et al. 1996; Bistolas & Hoffman 1998; Mathis et al. 2002; Klypin et al. 2003; Lavaux 2010). These challenges range from redshift-space distortions, shot-noise, galaxy bias, to finding the mapping between Eulerian and Lagrangian space.

Constrained simulations of the local universe have been already extensively used as a numerical near-field cosmological laboratory (for an overview see Gottlöber et al. 2010). The predictions of Warm and Cold Dark Matter cosmological models have been compared with the observed distribution of dwarfs in the Local Universe (Zavala et al. 2009; Tikhonov et al. 2009) and the reionisation history of the Local Group has been studied (Iliev et al. 2011). Zoomed high resolution simulations of the Local Group have been used to study the satellites of the Local Group galaxies (see e. g. Knebe et al. 2011; Libeskind et al. 2011; Knebe et al. 2011; di Cintio et al. 2011; Di Cintio et al. 2012), the formation of the Local Group (Forero-Romero et al. 2011) or recently the stripping of gas from dwarfs moving through the Local Web (see Benítez-Llambay et al. 2013).

The methods applied so far, need however a deep revision considering the recent theoretical advances and the acquisition of new data tracing the Local Universe. While the displacement field has been neglected in the works using velocity data (see e. g. Klypin et al. 2003), which are unbiased real-space tracers (see Bertschinger et al. 1990; Dekel et al. 1990; Zaroubi et al. 1999; Courtois et al. 2012), displacements have been considered within linear Lagrangian perturbation theory (Zel’dovich (1970) approximation) in most of the works using galaxy redshifts (Kolatt et al. 1996; Mathis et al. 2002). Nevertheless, treating in the latter case coherent redshift-space distortions in a very approximate way and thus leading to squashed structures perpendicular to the line of sight, as is apparent in the work of Mathis et al. (2002). A more sophisticated treat-

ment has been employed in Lavaux (2010) within the Zeldovich approximation, however lacking an analysis of the real-space reconstruction. An improvement may be achieved within this approximation from velocity data as well, as shown in Doumler et al. (2013). It has also been shown that higher order perturbation theory is significantly more precise than the Zeldovich approximation to estimate both the displacement and the velocity fields (see the pioneering works of Gramann (1993); Monaco & Efstathiou (1999); Narayanan et al. (2001); Mohayaee et al. (2003a, 2006) and more recent works on this subject in Kitaura & Angulo (2012); Kitaura et al. (2012); Neyrinck (2012); Kitaura & Heß (2012)).

Previous works used *inverse* approaches, in which either the smoothed density field (Nusser & Dekel 1992) or the galaxies (Peebles 1989; Nusser & Branchini 2000; Branchini et al. 2002; Brenier et al. 2003; Mohayaee et al. 2003b) are moved back in time according to the displacement field initially evaluated in Eulerian space, hereby effectively assuming a one-to-one relation in the Eulerian-Lagrangian mapping. This mapping is degenerate after shell-crossing and a statistical approach becomes necessary.

Alternative approaches have recently been proposed based on sampling the posterior distribution function of a Gaussian prior with a likelihood relating the initial fields with the observations through a particular structure formation model (see Kitaura 2013a; Jasche & Wandelt 2012; Wang et al. 2013) with its unprecedented application to observations in Kitaura et al. (2012).

We present in this work for the first time constrained  $N$ -body simulations using such a statistical *forward* approach based on observations. In particular we aim at reproducing the observed large-scale structure as it is traced by the distribution of galaxies in the Local Universe assuming hierarchical structure formation with  $\Lambda$ CDM cosmology and Gaussian seed fluctuations.

We have introduced many improvements with respect to previous techniques by using the recently developed Augmented Lagrangian Perturbation Theory (ALPT) structure formation model (see Kitaura & Heß 2012), and modelling redshift-space distortions taking into account the tidal shear tensor and including virialised motions (see Kitaura 2013b).

The quality of the constrained simulations which we present in this work permit us to reach a new level of precision, in which we can effectively consider them fully non-linear reconstructions of the large-scale structure. The set of simulations we obtain is highly correlated on large scales ( $\gtrsim 98\%$  with  $r_S = 3.5 h^{-1}$  Mpc), enabling us to study the influence of large scale modes on statistical processes (in a similar approach as Aragon Calvo 2013). The resemblance to the Local Universe makes it possible to directly compare the findings of the simulations with the observational data. The degree in which the observed distribution of matter is reproduced serves to test our cosmological models and verify our understanding of structure formation. A large variety of applications can be done based on these simulations with unprecedented accuracy, ranging from studies of the non-linear density and peculiar velocity fields, over galaxy bias analysis, to study merging histories and dependence on environment of particular objects.

The remainder of the paper is organised as follows. First we introduce the method, then we present the input data fol-

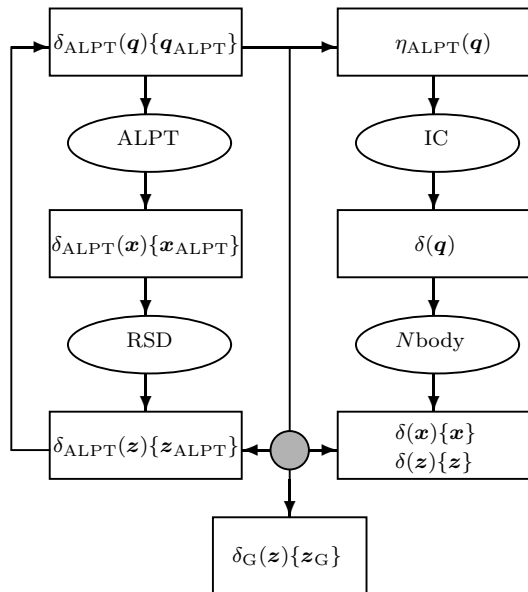


**Figure 1.** Methodology applied in this work. The left part of the flow-chart represents the KIGEN-code to find the large-scale primordial fluctuations. In an iterative self-consistent way the density fluctuations  $\delta(\mathbf{q}_{\text{ALPT}})$  are sampled at Lagrangian coordinates  $\{\mathbf{q}_{\text{ALPT}}\}$ . Structure formation is modelled within ALPT leading to the density field in Eulerian space  $\delta(\mathbf{x}_{\text{ALPT}})$ . Then redshift-space distortions (RSD) are added yielding  $\delta(\mathbf{z}_{\text{ALPT}})$ . A likelihood comparison (shaded circle) is done with the galaxy field  $\{\mathbf{z}_{\text{G}}\}$ . This process is iterated within a Gibbs- and Hamiltonian sampling scheme. The right part of the flow-chart shows the selection of samples according to their cross-correlation with the galaxy field and the subsequent generation of initial conditions (IC) for the  $N$ -body runs from the white-noise fields  $\eta_{\text{ALPT}}(\mathbf{q})$ . The results  $(\delta(\mathbf{x}), \delta(\mathbf{z}))$  are analysed and compared with the observations (shaded circle) to gain insights about our structure formation modelling and improve our reconstructions.

lowed by our constrained simulations and finally we discuss the results and present the conclusions.

## 2 METHOD

Our method consists of exploring in a self-consistent Bayesian based approach the Gaussian primordial fluctuations which after nonlinear cosmic evolution are compatible with the galaxy distribution. Here, approximate and efficient gravity solvers are needed. We then scan the large set of reconstructions to select the ones which show the largest correlation with the data. The corresponding set of Gaussian fields is resampled on a finer mesh to generate the initial conditions, which we finally use to perform high resolution constrained  $N$ -body simulations. These are employed to further confine the models used in the iterative scheme. Fig. 1 shows a flow-chart summarising the different steps in the method.

### 2.1 Assumptions

In our approach we assume that the primordial density fields are Gaussian distributed. Hence the two-point correlation

function fully characterises the statistics of the initial conditions. The corresponding power-spectrum is derived with CAMB (Lewis et al. 2000) using the WMAP7+BAO+h0 parameters (Komatsu et al. 2011) (for definiteness  $\Omega_{\Lambda} = 0.728$ ,  $\Omega_{\text{Matter}} = 0.272$ ,  $\Omega_{\text{Baryon}} = 0.046$ ,  $H_0 = 0.704$ , and  $\sigma_8 = 0.807$  and  $n_s = 0.967$ ). This cosmology is also used to evolve the density fields both in the reconstruction process using the approximate gravity solver (see §2.2.1) and in the constrained simulations using an  $N$ -body code. We assume that the density distribution in the Local Universe can be reproduced within the framework of  $\Lambda$ CDM cosmology and neglect for the time being baryonic physics. This will certainly play an important role at scales smaller than the Jeans length which is out of the scope of this work. Furthermore we assume periodic boundary conditions. This assumption is not critical, as the data considered here (see §3) are increasingly sparse towards the boundaries (the selection function drops to values of about  $10^{-2} - 10^{-3}$ ). While this will reduce the accuracy close to the boundaries, the inner regions are not affected considering that the correlation function of the density fluctuations quickly drops at distances larger than about  $10 h^{-1}$  Mpc. Peculiar velocities on the other hand can be correlated up to distances of about  $100 h^{-1}$  Mpc (see e. g. Erdoğan & Lahav 2009). Therefore, we will miss the external attractors to the volume considered in our work (see Hoffman 2000; Courtois et al. 2012, to add a posteriori the missing tidal component from velocity data). The details of the different models used in the reconstruction process can be found below.

### 2.2 Reconstruction of the large-scale primordial fluctuations

We rely on the KIGEN-code to recover the large-scale primordial fluctuations (Kitaura 2013a). The method implemented in this code is based on sampling Gaussian fields constrained by Lagrangian test particles  $\{\mathbf{q}\}$  (here Hamiltonian sampling is employed as developed in Jasche & Kitaura 2010; Kitaura et al. 2012), which after cosmic evolution (see 2.2.1) and once redshift-space distortions have been included (see 2.2.2) yields a distribution in Eulerian redshift-space  $\{\mathbf{z}\}$  compatible with the observed galaxies  $\{\mathbf{z}_{\text{G}}\}$ . The set of constraints (matter tracers on a grid) in Lagrangian space  $\{\mathbf{q}\}$  is obtained from the likelihood comparison between the particles in Eulerian redshift-space with the galaxies, as the information of each particle’s trajectory is known. Both quantities, the density fluctuations and the set of particles in Lagrangian space, are iteratively obtained within a Gibbs-sampling scheme (see Kitaura & Enßlin 2008, and references therein). Effectively we sample the posterior distribution function of Lagrangian density fields  $\delta(\mathbf{q})$  given a set of tracers in redshift-space  $\{\mathbf{z}_{\text{G}}\}$ , a structure formation model  $\mathcal{M}$  and a peculiar velocity field  $v$  which emerges from  $\mathcal{M}$ :  $P(\delta(\mathbf{q})|\{\mathbf{z}_{\text{G}}\}, \mathcal{M}, v)$  For more details on the method we refer to Kitaura (2013a,b).

#### 2.2.1 Structure formation model

In order to scan the parameter space of primordial fluctuations we need an efficient and computationally fast gravity solver. Most approximate structure formation models are inaccurate when shell-crossing becomes dominant, i. e. when

particles massively start crossing each others trajectories. Too severe shell-crossing can be prevented with the spherical collapse model (see Neyrinck 2012). However, one needs to take into account the tidal field component to be accurate on large-scales (see e. g. Scoccimarro & Sheth 2002). Therefore, we use the ALPT approach (see Kitaura & Heß 2012). This method is based on splitting the displacement field into a long- and a short-range component. The long-range component is computed by second order LPT (2LPT). This approximation contains a nonlocal and nonlinear tidal term. The short-range displacement field is given by a spherical collapse based solution. A Gaussian kernel with a smoothing radius of  $4 h^{-1}$  Mpc is used to separate between both regimes.

### 2.2.2 Redshift-space distortions treatment

Coherent redshift-space distortions are modelled within 2LPT. However, we consider two approaches to treat highly nonlinear redshift-space distortions.

- **CFOG:** The first being the widely used one in which the fingers-of-god (fogs) are compressed (see e. g. Erdoğdu et al. 2004; Tegmark et al. 2004a). We use a *friends-of-friends* algorithm taking into account the ellipsoidal distribution along the line-of-sight of groups of galaxies due to virial motions (see Tegmark et al. 2004b).

- **SFOG:** In the second approach we apply a novel sampling scheme (see Kitaura 2013b). We follow the ansatz proposed in Kitaura & Enßlin (2008) of splitting the velocity field into a coherent flow  $\mathbf{v}_r^{\text{coh}}$  and a dispersion term  $\mathbf{v}_r^\sigma$ :  $\mathbf{v}_r = \mathbf{v}_r^{\text{coh}} + \mathbf{v}_r^\sigma$  within the iterative reconstruction process (see also Kitaura et al. 2012). The dispersion term models the velocity distribution in closely virialised structures producing elongated structures along the line-of-sight. Here we use a density dependent dispersion and sample the redshift displacement from a Gaussian distribution (see Kitaura 2013b; Kitaura 2007).

We will compare both approaches against each other in our numerical calculations section (Sec. 4).

### 2.2.3 Galaxy bias

The galaxy bias which is effectively modelled within KI-GEN includes a nonlinear, nonlocal and a scale-dependent component. In the likelihood comparison step haloes are constructed at the positions of galaxies within the ALPT approximation with a friends-of-friends scheme (for a review on the halo-model see Cooray & Sheth 2002). A similar procedure was suggested for the 2LPT approximation by Scoccimarro & Sheth (2002) and applied in Manera et al. (2012). Further, in the posterior sampling step of Gaussian fields a scale dependent bias is effectively modelled. Hence even though matter tracers may pick up the galaxy bias, the Hamiltonian sampling process finds an unbiased Gaussian field.

The over-all shape of the power-spectrum is strongly determined by the prior correcting for a  $k$ -dependent bias. We will show in §4.3 that the characteristic features of the power-spectrum come from the particular matter distribution in the considered volume. Sampling the full shape of

the power-spectrum within the reconstruction process as suggested in Kitaura & Enßlin (2008); Jasche et al. (2010); Kitaura et al. (2012) is out of the scope in this work.

## 2.3 Scanning the posterior distribution function: selection of initial conditions

Once the Markov chain has converged it starts producing Gaussian fields sampled from the posterior probability distribution function (PDF). This enables us to compute various estimators like the mean of the posterior PDF yielding a smoothed conservative field (see Kitaura et al. 2010, 2012, and §4.3). We are, however, interested in samples which have the full power and at the same time can be considered as representative of the PDF. The mean properties of this subset should coincide with the corresponding mean of the full set having a smaller variance (see the case of peculiar motions in Kitaura et al. 2012). Therefore we select the set of primordial fluctuations which show the highest correlation with the galaxy field after cosmic evolution within a particular structure formation approximation. Here we choose a spectral analysis to estimate the degree of correlation between the dark matter (DM) reconstructions  $\delta_{\text{DM}}$  and the galaxy overdensity field  $\delta_{\text{G}}$ , i. e. the cross power-spectrum:

$$XP(k)[\delta_{\text{DM}}, \delta_{\text{G}}] \equiv \frac{\langle |\hat{\delta}_{\text{DM}}(\mathbf{k}) \hat{\delta}_{\text{G}}(\mathbf{k})| \rangle}{\sqrt{P_{\text{DM}}(k)} \sqrt{P_{\text{G}}(k)}}, \quad (1)$$

where the ensemble brackets denote angular averaging and  $P_{\text{DM}}(k)$  are  $P_{\text{G}}(k)$  the power-spectra corresponding to the fields  $\delta_{\text{DM}}$  and  $\delta_{\text{G}}$ , respectively. The matter overdensity field is defined by

$$\delta_{\text{DM}} \equiv \frac{N_{\text{DM}i}}{\bar{N}_{\text{DM}}} - 1, \quad (2)$$

where  $N_{\text{DM}i}$  denotes the number counts of simulated particles in cell  $i$  gridded with a clouds-in-cell (CIC) scheme, and  $\bar{N}_{\text{DM}}$  is the mean number counts computed dividing the total number of particles by the total number of cells in the considered volume. We define the galaxy overdensity by the maximum likelihood of a Poissonian distribution to compensate for selection function effects  $f_{\text{S}}$  (see e. g. Kitaura et al. 2009):

$$\delta_{\text{G}i} \equiv \frac{N_{\text{G}i}}{f_{\text{S}i} \bar{N}_{\text{G}}} - 1, \quad (3)$$

for each cell  $i$ , with the mean expected number counts being given by:  $\bar{N}_{\text{G}} \equiv \sum_i N_{\text{G}i} / f_{\text{S}i}$ . We impose a threshold  $XP_{\text{th}}$  at a given scale to filter out the tails of the posterior PDF and focus on the denser probability regions. Approaching the grid-resolution at high  $k$  the cross power-spectra start to fluctuate. Therefore we choose a value of  $k_{\text{th}}$  far below the Nyquist frequency ( $k_{\text{th}} = 1$ , see §4.2):

$$XP_{\text{ALPT,G}}^l(k = k_{\text{th}}) \equiv XP^l(k = k_{\text{th}})[\delta_{\text{ALPT}}, \delta_{\text{G}}] > XP_{\text{th}}, \quad (4)$$

for sample  $l$  in the Markov chain.

Cross power-spectra which satisfy this condition usually show higher correlations over the entire  $k$ -space region (see §4.2). To avoid selecting correlated samples, which are essentially identical, we discard first and second neighbours taking the largest correlated one among them:

$$XP_{\text{ALPT,G}}^l(k = k_{\text{th}}) > \max(XP_{\text{ALPT,G}}^{l-2} \dots^{l+2}(k = k_{\text{th}})). \quad (5)$$

## 2.4 Generation of high resolution initial conditions

From the set of primordial fluctuations we construct the corresponding white-noise fields:

$$\eta^l(\mathbf{k}) \equiv \frac{\hat{\delta}_q^l(\mathbf{k})}{\sqrt{P(k)}}, \quad (6)$$

for sample  $l$ , with  $P(k)$  being the theoretical linear power-spectrum and  $\delta_q$  standing for the overdensity field at the initial conditions in Lagrangian space  $q$ . We note that these fields are essentially uncorrelated from cell-to-cell, except for some residual deviations from a flat power-spectrum characteristic of the particular cosmic realisation. We checked that dividing  $\hat{\delta}_q^l(\mathbf{k})$  by the square root of the actual power-spectrum measured from the density field itself, i. e. with perfectly flat white-noise fields, leads to significantly less correlated density fields with the galaxy field after simulating structure formation. The construction of the white-noise field permits us to increase the resolution augmenting the smaller scales on a finer mesh randomly sampling from a Gaussian with unity variance. The resulting fields can then be multiplied in Fourier-space with the linear power-spectrum including modes up to the resampled scales. Here we assume the same cosmology as in the reconstruction algorithm to maximise the precision of the constrained simulations. From the resulting density fluctuations one needs to compute the displacement and velocities for the number of particles required in the  $N$ -body simulation. These steps are done within the initial conditions (ICs) generation code GINNUNGAGAP<sup>1</sup>, which is fully parallelised and has been extensively tested within the Zeldovich approximation.

## 2.5 Constrained $N$ -body simulations

The initial conditions computed as described in the previous sub-section are used to simulate structure formation with a  $N$ -body code. To avoid transients which could originate from the Zeldovich approximation in the generation of the ICs, we start the  $N$ -body simulations at a relatively high redshift of  $z = 100$ . We use GADGET-3, an improved version of the publicly available cosmological code GADGET-2 (last described in Springel 2005). The code is parallelised for distributed memory machines and uses a hierarchical tree algorithm for the calculation of gravity. We will restrict ourselves in this work to dark matter only  $N$ -body simulations and leave a detailed description of the star-forming, cooling and feedback processes for future work. The advantage of this step is that we can accurately model the nonlinear regime and get a realistic distribution of haloes. Haloes are defined in this context as spherical regions with a density higher than  $\rho > 200 \times \rho_{crit}$ , where  $\rho_{crit}$  is the critical density. To identify these regions we use the AHF-code<sup>2</sup> (Knollmann & Knebe 2009). The halo distribution can be used to further test the reconstruction algorithm and tune the models as we will show below (see §2.2 and §4.1).

## 3 INPUT DATA

Our input data in this work is the 2MASS redshift survey (2MRS),  $K_s = 11.75$  catalogue, with a median redshift of  $z \approx 0.028$  (Huchra et al. 2012). This catalogue provides an almost full sky observation of galaxy redshifts with a sky coverage of 91% and uniform completeness of 97.6% only limited by the presence of the foreground stars near the Galactic plane (*the Zone of Avoidance* (ZoA), where  $|b| < 5^\circ$  and  $|b| < 8^\circ$  near the Galactic centre). The same version of the augmented 2MRS catalogue was used as in Kitaura et al. (2012), which was filled in the ZoA with random galaxies generated from the corresponding longitude/distance bins in the adjacent strips (Yahil et al. 1991). This method is robust for the width of the 2MRS mask and has been thoroughly tested (for details see Erdoğan et al. 2006, and references therein).

The ZoA could be sampled with a Poissonian likelihood describing the counts-in-cells of the galaxy distribution which would be limited to a coarse grid resolution (see e.g. Kitaura et al. 2010). To incorporate a mask treatment within a particle based reconstruction method like KIGEN, we would need to sample mock galaxies (or haloes) according to our structure formation model following schemes like the one proposed in Scoccimarro & Sheth (2002), which is out of scope in this work.

We computed the selection function  $f_S$  directly based on the radial distribution galaxies ignoring the Kaiser-rocket effect (see Branchini et al. 2012).

A combination of reconstruction and simulation can only reproduce a density field as good as the data. Hence the stochasticity of galaxy formation and observational challenges obscure our insight in the true distribution of matter. Nevertheless due to quantity and precision of position measurements galaxy surveys are still the most detailed scan of density in the local universe.

## 4 NUMERICAL CALCULATIONS

In this study we focus on the Local Universe as comprised by a box of  $180 h^{-1}$  Mpc on a side with the observer located in the centre including 31017 2MRS galaxies (i. e. a number density of  $5.3 \cdot 10^{-3} (h^{-1} \text{Mpc})^{-3}$ ).

First we apply the KIGEN-code to find the large-scale primordial fluctuations. The resolution of the reconstruction is about  $1.4 h^{-1}$  Mpc on a mesh of  $128^3$  cells. We follow Kitaura et al. (2012) for the numerical setting of the KIGEN-code.

The number of constraints (=total number of cells  $\sim 2 \cdot 10^6$ ) used in the Hamiltonian sampling process (see Sec.2.2) is achieved by taking into account all volume elements including empty cells. Therefore we account for observed regions with no detections. This amount of information excels that of previous works which relied exclusively on the locations of density peaks (see Sec. 1) by about 2-3 orders of magnitudes. Even if one considers that peak positions are less correlated constraints than gridded volume elements, the latter obviously carries more information. The phase information is used without any additional smoothing to the gridding (see Wang et al. 2013, for smoothed constraints). This permits us to recover not only the density peaks, but

<sup>1</sup> publicly available at <https://code.google.com/p/ginnungagap/>

<sup>2</sup> publicly available <http://popia.ft.uam.es/AHF>

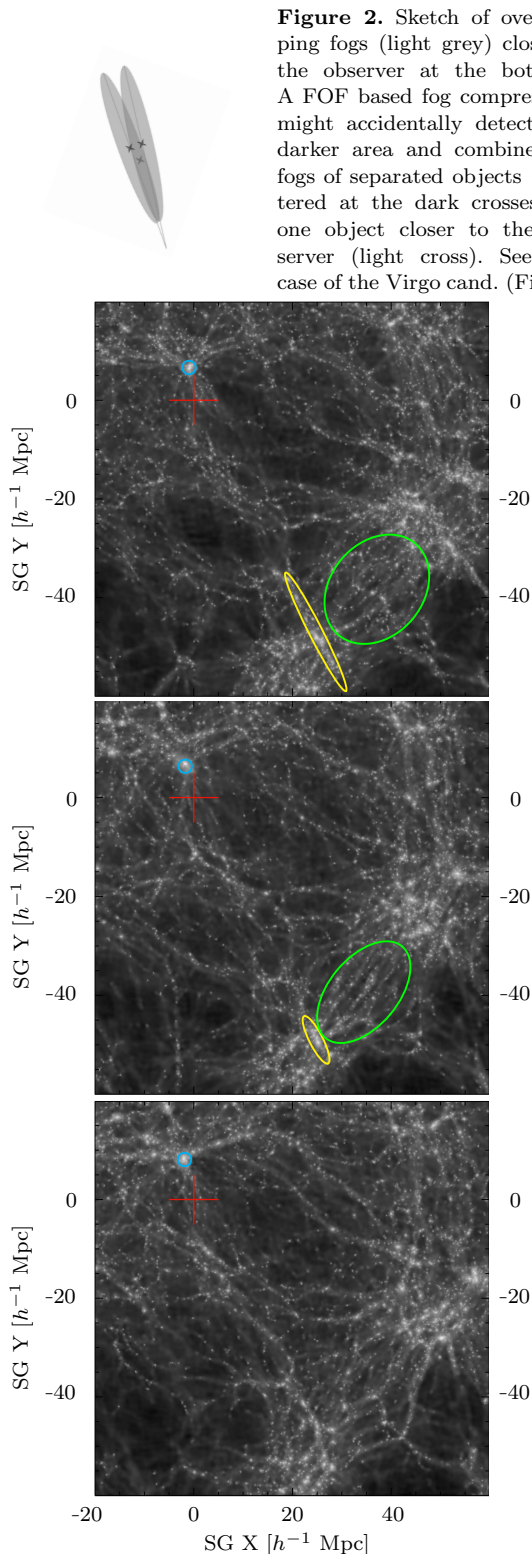


**Figure 3.** Artifacts due to shell-crossing and fog compression (CFOG). Logarithmic DM overdensity in real-space in a slice of  $22.5 h^{-1}$  Mpc thickness in the supergalactic XY plane. The panels correspond to a constrained simulation with (**top:**) 2LPT+CFOG, (**middle:**) ALPT+CFOG and (**bottom:**) ALPT+SFOG. The yellow ellipses show the negative fogs. The green highlighted area shows the *accordion*-effect, a preferential filament orientation perpendicular to the line-of-sight due to shell-crossing. The position of the Virgo cluster candidate (cyan circle) is shifted ( $2\text{--}3 h^{-1}$  Mpc) towards the observer (red cross) in the upper two panels w.r.t. the case shown in the lower panel.

**Figure 2.** Sketch of overlapping fogs (light grey) close to the observer at the bottom. A FOF based fog compression might accidentally detect the darker area and combine the fogs of separated objects (centered at the dark crosses) to one object closer to the observer (light cross). See the case of the Virgo cand. (Fig. 3)

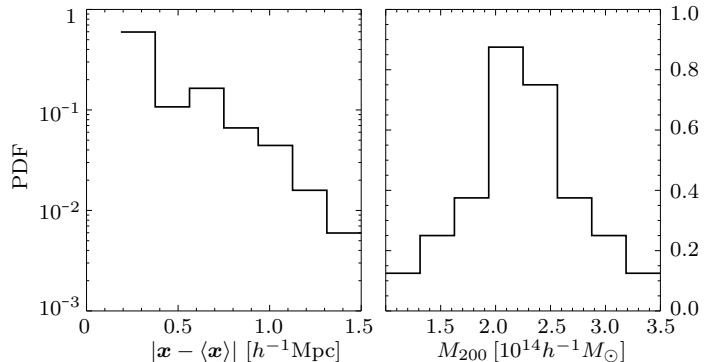


**Figure 4.** **Left panel:** PDF of finding the Virgo cluster candidate in the 25 constrained simulations (ALPT+SFOG) at a certain distance with respect to its mean position  $\langle \mathbf{x} \rangle$ . **Right panel:** corresponding mass PDF from the 25 simulations.

also filamentary structures as traced by the galaxy distribution (see §4.2).

The power-spectra of the subsequent primordial density fields in the Markov chain are unbiased with the theoretical linear power-spectrum on all scales as soon as the KIGEN-code has converged. For safety we consider samples after 2000 iterations for our study well after the previous criterion has been fulfilled. The Markov chain continues running to obtain a minimum of 1000 samples.

Our reconstructions based on 2LPT and the ALPT approximation using data with collapsed fogs (2LPT+CFOG and ALPT+CFOG, respectively) lead to constrained simulations with pronounced artifacts. These are caused by shell-crossing (see §4.1). As a consequence, the mass function of the case 2LPT-CFOG clearly deviated from the expected one based on random simulations. Therefore, we focus in this work on reconstructions using the ALPT structure formation model with the SFOG (ALPT+SFOG) prescription. We apply the full machinery sketched in Fig. 1 to perform constrained simulations. The simulations are conducted with  $384^3$  particles in a simulation box of  $180 h^{-1}$  Mpc per side which corresponds to a mass of  $7.8 \times 10^9 h^{-1} M_{\odot}$  of each mass element in the chosen cosmology. To this end we used a comoving gravitational softening of  $15 h^{-1}$  kpc.

Let us assess the quality of the constrained  $N$ -body simulations. We will first analyse our redshift-space distortions (RSD) treatment followed by a comparison with the observed galaxy field. Finally, we will compare the statistical properties of the CSs with a set of random simulations.

#### 4.1 Redshift-space distortions treatment

To investigate the accuracy of our SFOG treatment we compare it with the classical CFOG scheme following Tegmark et al. (2004a). The latter approach shows significantly larger correlations than the SFOG one. While the CFOG samples reach cross power-spectrum values of  $XP(k=1) \gtrsim 0.7$ , the SFOG ones remain at  $XP(k=1) \lesssim 0.5$ . The artificial collapse of fogs in the CFOG approach leads to relatively more clustered regions. This partially compensates for shell-crossing in the final density fields, and the corresponding lack of power of the approximate structure formation model. This effect can induce higher cor-



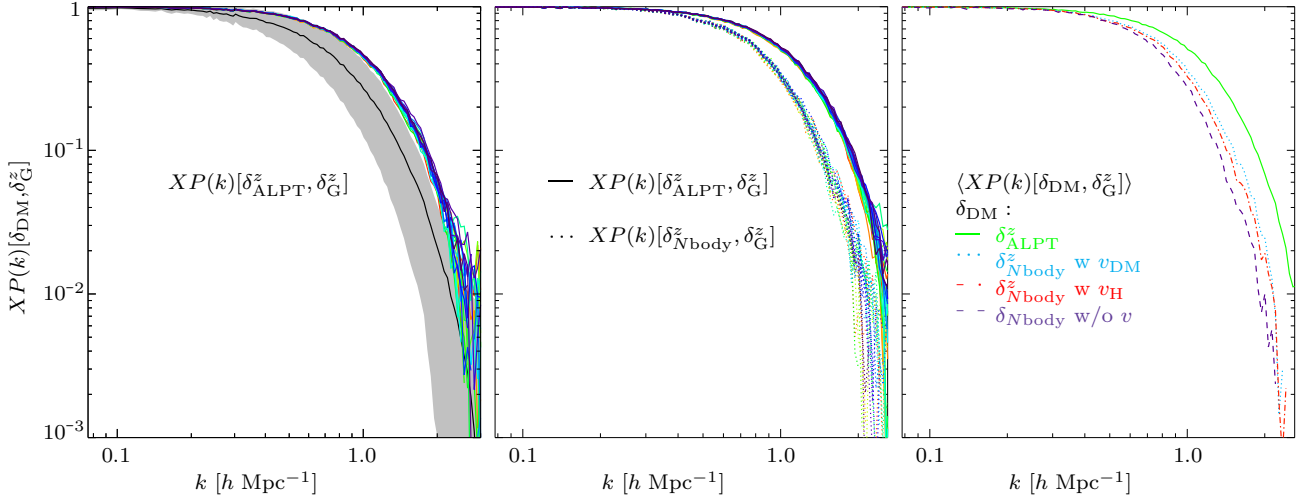


**Figure 5.** Cross power-spectra  $XP(k)$  between the DM reconstructions and the galaxy field. **Left panel:**  $XP(k)$  of a set of 1200 realisations corresponding to the ALPT+SFOG reconstructions. The shaded area denotes the standard deviation of the complete set. The coloured lines show a subset of 25 realisations that have been picked according to criterion 5. **Middle panel:** Cross power-spectra comparing the 2MRS galaxy overdensity with the ALPT overdensities of the 25 reconstructions (solid) and for their corresponding 25 constrained simulations (dotted). **Right panel:** Ensemble mean of the cross power-spectra between the galaxy field and the estimated dark matter field corresponding the ALPT reconstructions in redshift-space (solid green), the constrained simulations without RSD (dashed purple), with DM velocity based RSD (dotted blue) and with RSD based on Halo velocity fields (dash-dotted red).

relations. However, a deeper investigation, shows that the CFOG approach induces artifacts.

The first one comes from unfolding redshift-space to recover the real-space matter distribution. This happens in KIGEN in a forward approach, by adding redshift-space distortions to the simulated particles in the likelihood comparison step (see Kitaura 2013a). A correct modelling of RSD is therefore necessary to obtain accurate reconstructions. One of the problems of using an approximate structure formation model based on perturbation theory is that the highly nonlinear virialised motions are not included. As shown in Hamilton (1998) coherent redshift-space distortions can already produce fogs. Galaxies coherently approaching each other in a potential well, would produce shell-crossing in redshift-space due to their peculiar motions, leading to elongated structures. Since in the CFOG case KIGEN tries to match the compressed data, negative fogs appear in real-space. This effect is boosted with artificial shell-crossing, as can be seen when using the 2LPT approximation (see fogs in real-space in the upper two panels of Fig. 3, where we zoomed into an area of  $80 h^{-1} \text{Mpc}$ ). Treating only coherent fogs also fans out parallel filamentary structures like an *accordion*, as is apparent in the green highlighted areas in Fig. 3. One can see in the extension of the parallel filamentary structures that shell-crossing is more severe with 2LPT than ALPT (compare green areas). Another important aspect is the uncertainty in the location of the mass distribution in high density regions. While the CFOG scheme ignores this point yielding a single solution, the SFOG sampling approach propagates the uncertainty in each Markov chain sample. A fogs compressed based reconstruction is therefore underestimating the uncertainty in high density regions. Moreover, the CFOG compression produces systematic artificial displacements of clusters located close to the observer. This situation is depicted in Fig. 2. In regions where var-

ious fogs overlap it is difficult to find the centres of mass with friends-of-friends algorithm. We found that clusters in such fogs are systematically located closer to the observer. Galaxies residing in the distant tails of fogs, which are more separated, may not be considered *friends* and hence a single shorter fog is detected with its centre closer to the tails where the fogs converge, i. e. closer to the observer. This is the case of the local super cluster which includes Virgo. Fig. 3 shows the location of our Virgo candidate (massive cluster within the cyan circle) with respect to the observer (red cross) with both schemes. We find that the position of the Virgo candidate is estimated to be about  $2.5 h^{-1} \text{Mpc}$  closer to the observer with the CFOG scheme than with the SFOG one (distances of  $6.8 h^{-1} \text{Mpc}$  and  $9.3 h^{-1} \text{Mpc}$  respectively for the ensemble means of 25 simulations each).

The robustness of the RSD treatment can be seen in the uncertainty of the position of particular objects. The spread in distance of the Virgo candidate across all 25 ALPT+SFOG constrained simulations is very small ( $1 \sigma < 1 h^{-1} \text{Mpc}$ ), as shown in Fig. 4. Also the mass of the corresponding object is strongly constrained as shown in the right panel. This indicates that a constrained environment leads to a constrained final mass of halos. We plan to investigate this further and plan to study the mass evolution of particular objects and the influence of the environment.

It is possible to improve the SFOG scheme in various ways. The description of coherent velocities should be revised. Furthermore, a radial dependent dispersion velocity needs to be implemented to account for observational selection effects, as we plan to do in future work. Nevertheless, the SFOG approach as presented in this work leads to constrained simulations, which solve many of the problems present with the common CFOG scheme to great extent. For this reason we will restrict from now on our study to the set of 25 ALPT+SFOG based constrained simulations.

## 4.2 Comparison with the observations

The cross power-spectra between the ALPT reconstructions with the SFOG treatment and the galaxy field are shown on the left panel in Fig. 5. They present very high values up to  $k \sim 1 h \text{Mpc}^{-1}$  and are still correlated at  $2.2 < k < 3 h \text{Mpc}^{-1}$  ( $1 \sigma$  area of the zero crossing of the cross power-spectra). The exact value of the zero crossing of the cross-powerspectrum of a single simulation inhibits some stochasticity, due to weak (anti-)correlations of random modes at the transition-scale from constrained to random. Such incidents of matching phases are present in all correlations of random fields. However by investigating the ensemble of simulations we are able to quantify this random process and we are able to specify this 68% C.I.

We select the 25 most correlated samples represented by the different coloured lines as shown in Fig. 5. Those samples, which are higher correlated with the galaxy field at a given  $k$ , show in most of the cases higher correlations in the entire  $k$ -space. Such a rank-ordered behaviour is broken in some cases when approaching the Nyquist frequency at  $k \gtrsim 2 h \text{Mpc}^{-1}$ . This demonstrates the robustness of our selection approach focusing at  $k = 1 h \text{Mpc}^{-1}$  (see §2.3). The required threshold at  $k = 1$  to select the 25 samples was:  $XP_{\text{th}} = 0.43$ . By focusing only on the best correlated reconstructions we do not sample the full parameter space of primordial density fluctuations, but focus on the regions which are best correlated in the reconstructions. The middle panel of Fig. 5 shows the cross power-spectra corresponding to the  $N$ -body simulations, being systematically less correlated as compared to the ALPT ones. The reason for this is that the initial conditions have essentially been computed within the ALPT approximation in addition to a particular peculiar velocity model (2LPT with a dispersion term) to simulate RSD. The  $N$ -body solutions (modelling gravity more accurately) do not fully agree with these models and introduce a small displacement. It would thus be interesting to include in the future full gravity solvers within the reconstruction process. In the right panel we demonstrate that our RSD treatment is over-all correct yielding higher correlations when transforming the simulation from real-space (violet curve) into redshift-space (cyan and red curves). Here we consider two ways of transforming the data, using the peculiar velocities of the dark matter particles in one case (cyan) and the ones of the halo in the other (red). The right panel in Fig. 5 demonstrates that our RSD modelling is over-all correct as the cross-power spectra are clearly higher when including redshift-space distortions. The lower correlation when using the halo velocity fields is due to the additional stochastic process of collapsing objects along the line-of-sight. The larger dispersion when taking the DM velocities enhances the probability that a number of simulated particles match the positions of observed galaxies. Nevertheless, matter is distributed in a more realistic manner using the halo velocity fields as we will discuss below. We would like to emphasise that we take the galaxy field according to Eq. 3 including redshift-space distortions (also fogs) in our cross-correlation analysis.

To further assess the quality of the constrained simulations we make a cell-to-cell comparison between the simulated and the observed density fields in configuration space. The correlation between two fields  $\phi_1$  and  $\phi_2$  can be quan-

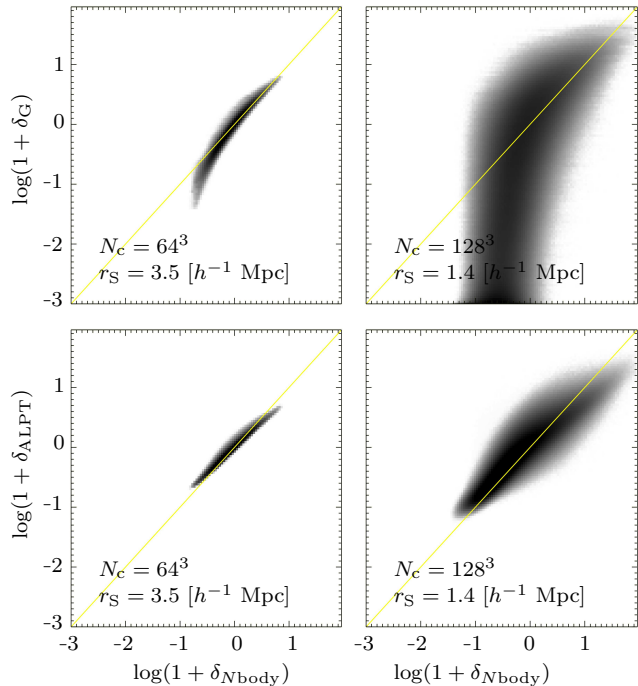


**Figure 6.** Two dimensional histogram of a cell-to-cell comparison in logarithmic-space including RSD (based on the halo velocity field) between the constrained simulations and the **(top:)** 2MRS galaxy field; **(bottom:)** ALPT+SFOG reconstructions. A CIC algorithm was used with **(left:)**  $64^3$  cells and Gaussian smoothing with  $r_S = 3.5 h^{-1} \text{Mpc}$ ; **(right:)**  $128^3$  cells and  $r_S = 1.4 h^{-1} \text{Mpc}$  (cell width). Note that in this resolution most of the cells don't contain galaxies. Underdense cells in the Nbody simulation are therefore matched with (almost) empty cells in the galaxy field. Darker grey-scale indicates a larger number of cells.

tified through the Pearson correlation coefficient  $r$

$$r(\phi_1, \phi_2) = \frac{\sum_i (\phi_{1i} - \bar{\phi}_1) (\phi_{2i} - \bar{\phi}_2)}{\sqrt{\left(\sum_i (\phi_{1i} - \bar{\phi}_1)\right)^2 \left(\sum_j (\phi_{2j} - \bar{\phi}_2)\right)^2}}. \quad (7)$$

Let us focus here on the logarithmic overdensity  $\phi \equiv \ln(1 + \delta)$  for various reasons: first this representation yields an estimate of the linear density field component (see Neyrinck et al. 2009; Kitaura & Angulo 2012); second it suppresses shot-noise in overdense areas<sup>3</sup>.

Fig. 6 shows the average cell-to-cell correlation between the  $N$ -body simulations and the galaxy field, and respectively ALPT, in different grid resolutions as compared to the ALPT reconstructions. We find that the uncertainty is much larger in the underdense regions, as can be seen in the increasing scatter towards negative values. The close alignment with the 45° slope in the upper panels demonstrates that the galaxy bias is very close to unity, especially on scales larger than  $r_S = 3.5 h^{-1} \text{Mpc}$ . The deviations from the 45°

<sup>3</sup> Let us write the galaxy overdensity field as the sum of the expected galaxy density field and the shot-noise term:  $\delta_G = \delta_G^{\text{exp}} + \epsilon$  (see Kitaura et al. 2010). The residual shot-noise term is accordingly given in the logarithmic representation by:  $\ln(1 + \delta_G) - \ln(1 + \delta_G^{\text{exp}}) = \ln\left(1 + \frac{\epsilon}{1 + \delta_G^{\text{exp}}}\right)$ .



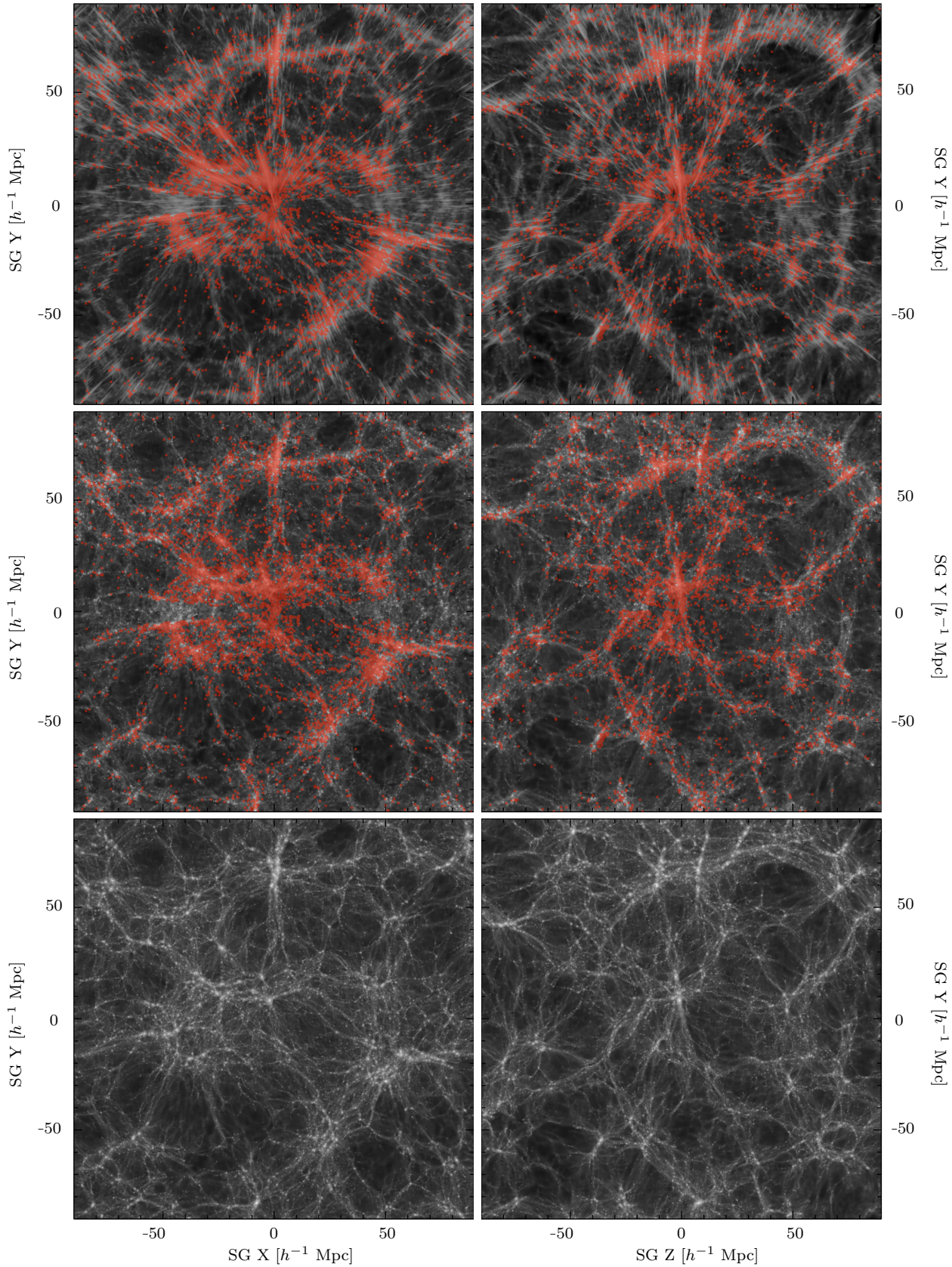


**Figure 7.** Density fields in supergalactic coordinates. **Upper panels: redshift-space.** Logarithmic DM overdensity of one of our constrained simulations (based on ALPT+SFOG) in a slice of  $22.5 h^{-1}$  Mpc thickness in supergalactic coordinates XY around  $Z=0$  (left) and ZY around  $X=0$  (right). Redshift-space distortions have been computed according to the DM particle velocities. The overdensity maps have been blended with the distribution of galaxies (red dots). **Middle panels: redshift-space.** Same as upper panels, but taking the halo velocity field. **Lower panels: real-space.** Same as upper panels without galaxies. The densities have been calculated with a SPH-kernel fixed to 32 neighbours.

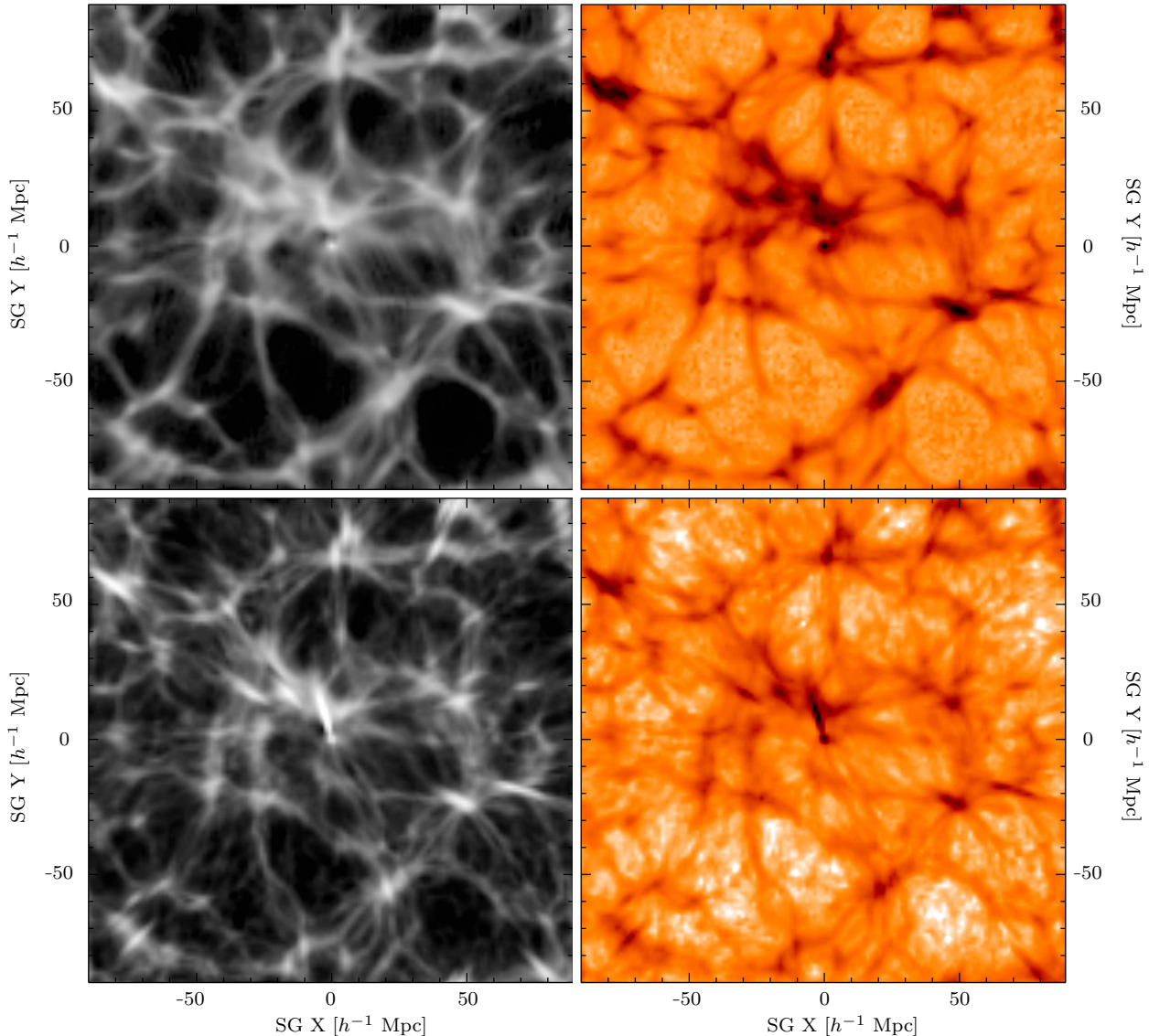


**Figure 8.** Signal and signal-to-noise maps in the supergalactic XY plane. **Left panels:** Ensemble-averaged logarithm of the overdensity fields ( $\langle \log(\rho/\bar{\rho}) \rangle$ ) of ALPT+SFOG reconstructions (top) and constrained simulations (bottom) showing the middle slice of a  $128^3$  CIC-grid. **Right panels:** Ensemble-averages divided by the standard deviation of the ensemble of reconstructions (top) and simulations (bottom) see Eq. 8.

slope shown in the lower panels are due to the perturbative approach of the ALPT approximation, which does not fully capture the nonlinear behaviour of gravitational clustering (see Kitaura & Heß 2012).

The corresponding cross-correlation coefficients are very high, being  $r = 98.3 \pm 0.1 \%$  on smoothing scales of  $r_S = 3.5 h^{-1}$  Mpc for both the ALPT reconstructions and the constrained simulations. For  $r_S = 1.4 h^{-1}$  Mpc we get  $r = 78.6 \pm 0.3 \%$  and  $73.8 \pm 0.1 \%$ , respectively.

Interestingly, if we keep the constrained simulations in real-space, we still obtain  $r = 97.5 \pm 0.1 \%$  with  $r_S = 3.5 h^{-1}$  Mpc for the cross-correlation between the galaxy field (in redshift-space). This tells us that small changes in  $r$  of  $\sim 1\%$  with  $r_S = 3.5 h^{-1}$  Mpc can imply improvements in the precision of the reconstruction of the order of  $\sim 5 h^{-1}$  Mpc (the order of coherent RSD). Such an estimation is important when comparing with previous works (see Lavaux 2010,

where a value of  $r = 97\%$  is obtained taking a smaller volume made by a sphere with a radius of  $60 h^{-1}$  Mpc and a volume limited 2MRS galaxy field using the same  $r_S$ ).

Fig. 7 visualises the accuracy of the constrained simulation by plotting on top of the dark matter density field the distribution of galaxies. It is remarkable how accurately the red dots, each one standing for a galaxy, match the simulated structures in redshift-space. The constrained simulations are even able to connect filaments traced by a few galaxies. The upper panels show the maps using the DM velocities, while the middle ones are based on the halo velocity field. For definiteness we move the simulation particles according to the velocity of their host halo if available. For non virialised particles we use the halo velocity field on a grid of  $128^3$ . We can clearly see that in the upper panels fogs are overestimated. Structure formation forms bound objects, therefore the correct way of modelling RSD consists of tak-



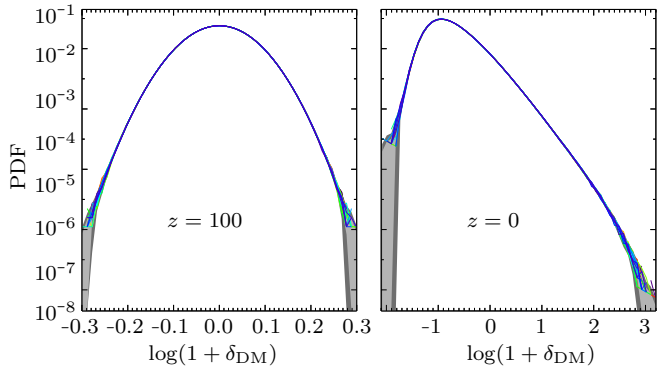


**Figure 9.** Matter statistics. **Left panel:** Matter PDF of the 25 constrained simulations (same colour-code as Fig. 5) at initial redshift  $z = 100$ . **Right panel:** same as left panel but at final time  $z = 0$ . The light and dark grey shaded contours indicate 1 and 2 sigma regions according to the 25 random simulations.

ing the halo velocity field to transform the simulation from real-space to redshift-space. To accurately model the RSD one needs a high enough resolution to resolve the masses of the observed objects and consider selection effects. The velocity dispersion of galaxies decreases with distance to the observer, since magnitude cuts tend to select more massive objects at increasing distances. We plan to perform a study of high resolution  $N$ -body simulations to study this in detail. Our current simulations yield already realistic fogs, as can be seen from the middle panels in Fig. 7. The lower panels in that figure show a *natural* real-space matter distribution with more extended structures along the line-of-site as opposed to the squashed structures in redshift-space (see Coma, Great Attractor and Perseus-Pisces region). Here we also find that the Local Void is less empty than it appears in redshift-space.

### 4.3 Statistical analysis

Here we want to investigate the robustness of the constrained simulations by looking at their statistical properties. Fig. 8 shows in the left panels the ensemble-averaged densities in logarithmic space  $\langle \log(\delta + 1) \rangle = \langle \log(\rho/\bar{\rho}) \rangle$  corresponding to the set of ALPT reconstructions and simulations. This demonstrates the consistency between the ALPT and the  $N$ -body simulations on scales larger than a few Mpc confirming our cell-to-cell comparison. However the  $N$ -body simulations show as expected, much more small-scale power. Looking at the signal-to-noise ratio:

$$\frac{S}{N} \equiv \frac{\langle \log(1 + \delta_{\text{DM}}) \rangle}{\sqrt{\langle (\log(1 + \delta_{\text{DM}}))^2 \rangle - \langle \log(1 + \delta_{\text{DM}}) \rangle^2}}, \quad (8)$$

where the ensemble mean is computed by volume averaging, we find that the uncertainty is smaller (darker colours) for the ALPT case. The small-scale power in the  $N$ -body case can be especially seen in the larger uncertainties in low density regions.

To accurately assess the statistical quality of the constrained simulations we construct a reference sample of 25 randomly seeded  $N$ -body simulations with the same setup.

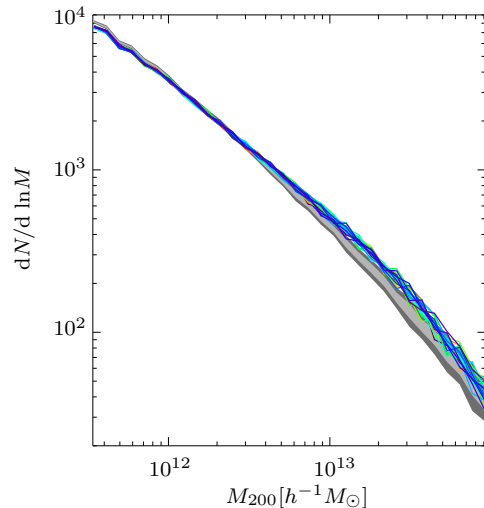


**Figure 10.** Mass function  $N(M)$  of halos in the ensemble of 25 constrained simulations (same colour-code as Fig. 5). The light and dark grey shaded contours indicate 1 and 2 sigma regions according to the 25 random simulations.

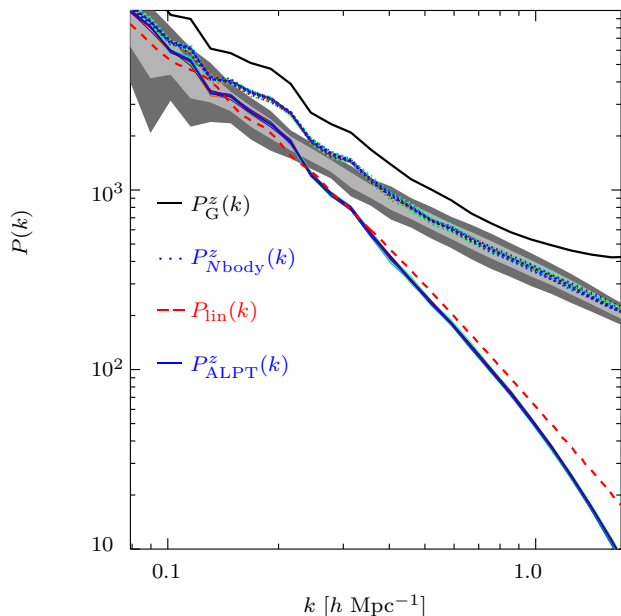


**Figure 11.** Power-spectra of the 2MRS galaxy overdensity (black) the ALPT+SFOG reconstructions in real sapce (coloured solid), and the constrained simulations in real space (coloured dotted). The light and dark grey shaded contours indicate 1 and 2 sigma regions according to the 25 random simulations.

We checked that the white-noise fields used for the initial conditions have numerically vanishing statistical moments: mean, skewness and kurtosis. Fig. 9 shows the matter statistics for the constrained simulations at redshifts 100 and 0. We find that the curves lie within the variance of the reference random simulations. The mass function (Fig. 10) shows a slight overproduction of massive haloes for the mass range  $M_{200} > 10^{13} h^{-1} M_{\odot}$ , being, however, compatible with the reference set within the error bars. It is unclear, whether

the particular realisation of the observed volume could be responsible for this issue.

Finally, we analyse the power-spectra to verify the method and the quality of the constrained simulations. This is shown in Fig. 11. Here one can see that the specific features of the galaxy power-spectrum, characteristic of the particular matter distribution, are preserved both in the ALPT reconstructions and in the constrained simulations. We can also see that the CSs have more power than the ALPT reconstructions, correcting for the bias caused by the perturbative structure formation approach. The black solid line shows the excess of power for the galaxy field due to the galaxy bias and shot-noise. The solid lines show the strongly biased nature of the ALPT+SFOG model. The constrained simulations however, are close to unbiased with respect to the random simulations and show the characteristic features of the particular realisation of the Local Universe. Fig. 11 demonstrates that we are reasonably modeling, in a scale dependent way, the biased nature of the galaxy field and the nonlinear gravitational clustering up to high  $ks$  ( $k \gtrsim 2 h \text{ Mpc}^{-1}$ ).

## 5 CONCLUSIONS

We have presented in this work constrained  $N$ -body simulations of the Local Universe based on the 2MRS galaxy redshift catalogue. This is the first time that a statistical self-consistent *forward* approach is applied to observations to obtain the fully nonlinear phase-space distribution. Our approach is based on sampling the posterior distribution function of a Gaussian prior with a likelihood relating the initial fields with the observations through a particular structure formation model. In this way we can exploit the high number density of observed galaxies in the Local Universe and use between 2 and 3 orders of magnitude more constraints for the initial fields than previous works. Special care has been taken to include recent improvements in modelling structure formation and redshift-space distortions within the reconstruction method of the primordial fluctuations. In particular, Augmented Lagrangian Perturbation Theory (ALPT) was used and redshift-space distortions were modelled, hence taking into account the tidal shear tensor and including the modelling of virialised motions.

Our studies have shown, that this effort is necessary to deal with such a large number of constraints, while resolving the density field down to scales of 2-3  $h^{-1} \text{ Mpc}$ . Otherwise, strong artifacts are introduced in the constrained simulations due to transients which originated through shell-crossing in the iterative reconstruction process. We verified that this is the case, when using standard second order Lagrangian perturbation theory or when using the galaxy distribution where the fingers-of-god have been collapsed. Parallel filamentary structures perpendicular to the line-of-sight and negative fingers-of-god in real-space appear in such cases. We also found that the position of clusters which are distorted as fingers-of-god close to the observer (such as Virgo) tend to be systematically closer in the collapsing schemes. We have managed to strongly suppress all these effects with our improved treatments. Nevertheless, we consider that further investigation should be carried out improving the models with respect to the statistical properties

of the constrained simulations. One focus should be on the mass functions. We found, that those show a slight overproduction of massive haloes, which may or may not be induced by an artifact. This is not clear, as the deviation is small and can be considered compatible with the random simulations. Especially so since one must also consider that the Local Universe is a particular realisation, which could have very specific statistical characteristics. Nevertheless the compatibility between the constrained simulations and the random ones in the matter statistics at starting and final redshifts and in the power-spectra, demonstrates the quality of the constrained simulations. Certainly, we should improve our selection function treatment, including a real-space estimation to treat the Kaiser-rocket effect. We have considered that this is negligible given the small volume we are studying. In any case, such an improvement would also permit us to tackle larger volumes for which the selection function drops more dramatically. In those studies one could also investigate the peculiar motions on larger scales, including more distant attractors, since now we are limited by the size of the box ( $180 h^{-1} \text{ Mpc}$ ) and the periodic boundary conditions.

This work serves as a consistency check for our understanding of structure formation. In this sense the high level of resemblance between our models and the actual galaxy distribution corroborate the initial assumptions and therefore do not indicate any deviations from the standard cosmological model. It would be interesting to extend this kind of study varying the assumptions to further test our models and verify whether these are the most compatible with observations. The level of precision that we achieve already in this work should help to get new insights into fields of study that require accurate density estimates of the Local Universe such as cosmic rays, the warm hot inter-galactic medium or Dark Matter annihilation and decay signals. The full nonlinear velocity field determined in this work can contribute to our understanding of the cosmic flows in the Local Universe. Furthermore the simulations can also provide a consistent formation history of particular clusters. We plan to exploit this by studying objects within their correct environment, explore their formation histories and compare them with observations.

## ACKNOWLEDGEMENTS

The authors thank the CLUES collaboration<sup>4</sup>, in particular Yehuda Hoffman, Gustavo Yepes and Timur Doumler for very encouraging and helpful discussions. Special thanks to Arman Khalatyan for providing us with the friends-of-friends code, Steffen Knollmann for assistance with GINNINGAGAP, Pirin Erdođdu for providing us the augmented 2MRS catalogue. SH acknowledges support by the Deutsche Forschungsgemeinschaft under the grant GO563/21 – 1.

<sup>4</sup> [www.clues-project.org](http://www.clues-project.org)

## REFERENCES

- Alimi J.-M., Bouillot V., Ramera Y., Reverdy V., Corasaniti P.-S., Balmes I., Requena S., Delaruelle X., Richet J.-N., 2012, ArXiv e-prints 1206.2838
- Angulo R. E., Springel V., White S. D. M., Jenkins A., Baugh C. M., Frenk C. S., 2012, MNRAS, 426, 2046
- Aragon Calvo M. A., 2013, in American Astronomical Society Meeting Abstracts Vol. 221 of American Astronomical Society Meeting Abstracts, Local Ensemble N-body Simulations: Generating Multiple Local Paths of Galaxy Formation. p. 132.04
- Benítez-Llambay A., Navarro J. F., Abadi M. G., Gottlöber S., Yepes G., Hoffman Y., Steinmetz M., 2013, ApJ, 763, L41
- Bertschinger E., 1987, ApJ, 323, L103
- Bertschinger E., Dekel A., Faber S. M., Dressler A., Burstein D., 1990, ApJ, 364, 370
- Bistolas V., Hoffman Y., 1998, ApJ, 492, 439
- Branchini E., Davis M., Nusser A., 2012, ArXiv e-prints 1202.5206
- Branchini E., Eldar A., Nusser A., 2002, MNRAS, 335, 53
- Brenier Y., Frisch U., Hénon M., Loeper G., Matarrese S., Mohayaee R., Sobolevskii A., 2003, MNRAS, 346, 501
- Cooray A., Sheth R., 2002, Physics Reports, 372, 1
- Courtois H. M., Hoffman Y., Tully R. B., Gottlöber S., 2012, ApJ, 744, 43
- Davis M., Efstathiou G., Frenk C. S., White S. D. M., 1985, ApJ, 292, 371
- Dekel A., Bertschinger E., Faber S. M., 1990, ApJ, 364, 349
- Di Cintio A., Knebe A., Libeskind N. I., Brook C., Yepes G., Gottloeber S., Hoffman Y., 2012, ArXiv e-prints 1204.0515
- di Cintio A., Knebe A., Libeskind N. I., Yepes G., Gottlöber S., Hoffman Y., 2011, MNRAS, 417, L74
- Doumler T., Gottlöber S., Hoffman Y., Courtois H., 2013, MNRAS, p. 628
- Erdoğan P., Huchra J. P., Lahav O., Colless M., Cutri R. M., Falco E., George T., Jarrett T., et al 2006, MNRAS, 368, 1515
- Erdoğan P., Lahav O., 2009, Phys. Rev. D, 80, 043005
- Erdoğan P., Lahav O., Zaroubi S., Efstathiou G., Moody S., Peacock J. A., Colless M., Baldry I. K., et al. 2004, MNRAS, 352, 939
- Forero-Romero J. E., Hoffman Y., Yepes G., Gottlöber S., Piontek R., Klypin A., Steinmetz M., 2011, MNRAS, 417, 1434
- Fry J. N., Peebles P. J. E., 1978, ApJ, 221, 19
- Gottlöber S., Hoffman Y., Yepes G., 2010, ArXiv e-prints 1005.2687
- Gramann M., 1993, ApJ, 405, 449
- Hamilton A. J. S., 1998, in Hamilton D., ed., The Evolving Universe Vol. 231 of Astrophysics and Space Science Library, Linear Redshift Distortions: a Review. pp 185–+
- Hoffman Y., 2000, in Courteau S., Willick J., eds, ASP Conf. Ser. 201: Cosmic Flows Workshop Eigenmode Analysis of Radial Velocities. pp 215–+
- Hoffman Y., Ribak E., 1991, ApJ, 380, L5
- Huchra J. P., Macri L. M., Masters K. L., Jarrett T. H., Berlind P., Calkins M., Crook A. C., Cutri R., Erdoğan P., Falco E., George T., Hutcheson C. M., Lahav O., Mader J., 2012, Rev.Astrn.Astrophys., 199, 26
- Iliev I. T., Moore B., Gottlöber S., Yepes G., Hoffman Y., Mellema G., 2011, MNRAS, 413, 2093
- Jasche J., Kitaura F.-S., 2010, MNRAS, 407, 29
- Jasche J., Kitaura F.-S., Wandelt B. D., Enßlin T. A., 2010, MNRAS, 406, 60
- Jasche J., Wandelt B. D., 2012, ArXiv e-prints 1203.3639
- Kim J., Park C., Gott III J. R., Dubinski J., 2009, ApJ, 701, 1547
- Kitaura F.-S., 2007, PhD thesis, Ludwig-Maximilians Universität München
- Kitaura F.-S., 2013a, MNRAS, 429, L84
- Kitaura F.-S., Angulo R. E., 2012, MNRAS, 425, 2443
- Kitaura F.-S., Angulo R. E., Hoffman Y., Gottlöber S., 2012, MNRAS, 425, 2422
- Kitaura F.-S., Enßlin T. A., 2008, MNRAS, 389, 497
- Kitaura F.-S., Erdoğan P., Nuza S. E., Khalatyan A., Angulo R. E., Hoffman Y., Gottlöber S., 2012, MNRAS, 427, L35
- Kitaura F.-S., Gallerani S., Ferrara A., 2012, MNRAS, 420, 61
- Kitaura F.-S., Heß S., 2012, ArXiv e-prints 1212.3514
- Kitaura F.-S., Jasche J., Li C., Enßlin T. A., Metcalf R. B., Wandelt B. D., Lemson G., White S. D. M., 2009, MNRAS, 400, 183
- Kitaura F.-S., Jasche J., Metcalf R. B., 2010, MNRAS, 403, 589
- Kitaura F.-S. e. a., 2013b, in prep.
- Klypin A., Hoffman Y., Kravtsov A. V., Gottlöber S., 2003, ApJ, 596, 19
- Knebe A., Libeskind N. I., Doumler T., Yepes G., Gottlöber S., Hoffman Y., 2011, MNRAS, 417, L56
- Knebe A., Libeskind N. I., Knollmann S. R., Martinez-Vaquero L. A., Yepes G., Gottlöber S., Hoffman Y., 2011, MNRAS, 412, 529
- Knollmann S. R., Knebe A., 2009, Rev.Astrn.Astrophys., 182, 608
- Kolatt T., Dekel A., Ganon G., Willick J. A., 1996, ApJ, 458, 419
- Komatsu E., et al., 2011, Astrophys.J.Suppl., 192, 18
- Kuhlen M., Vogelsberger M., Angulo R., 2012, Physics of the Dark Universe, 1, 50
- Lavaux G., 2010, MNRAS, 406, 1007
- Lewis A., Challinor A., Lasenby A., 2000, Astrophys. J., 538, 473
- Libeskind N. I., Knebe A., Hoffman Y., Gottlöber S., Yepes G., Steinmetz M., 2011, MNRAS, 411, 1525
- Manera M., Scocimarro R., Percival W. J., Samushia L., McBride C. K., Ross A. J., Sheth R. K., et al. 2012, MNRAS, p. 118
- Mathis H., Lemson G., Springel V., Kauffmann G., White S. D. M., Eldar A., Dekel A., 2002, MNRAS, 333, 739
- Mohayaee R., Frisch U., Matarrese S., Sobolevskii A., 2003a, Astr.Astrophys., 406, 393
- Mohayaee R., Frisch U., Matarrese S., Sobolevskii A., 2003b, Astr.Astrophys., 406, 393
- Mohayaee R., Mathis H., Colombi S., Silk J., 2006, MNRAS, 365, 939
- Monaco P., Efstathiou G., 1999, MNRAS, 308, 763
- Narayanan V. K., Weinberg D. H., Branchini E., Frenk C. S., Maddox S., Oliver S., Rowan-Robinson M., Saunders W., 2001, Rev.Astrn.Astrophys., 136, 1
- Neyrinck M. C., 2012, ArXiv e-prints 1204.1326



- Neyrinck M. C., Szapudi I., Szalay A. S., 2009, *ApJ*, 698, L90
- Nusser A., Branchini E., 2000, *MNRAS*, 313, 587
- Nusser A., Dekel A., 1992, *ApJ*, 391, 443
- Park C., Choi Y.-Y., Kim J., Gott III J. R., Kim S. S., Kim K.-S., 2012, *ApJ*, 759, L7
- Peebles P. J. E., 1989, *ApJ*, 344, L53
- Prada F., Klypin A. A., Cuesta A. J., Betancort-Rijo J. E., Primack J., 2012, *MNRAS*, 423, 3018
- Scoccimarro R., Sheth R. K., 2002, *MNRAS*, 329, 629
- Springel V., 2005, *MNRAS*, 364, 1105
- Springel V., White S. D. M., Jenkins A., Frenk C. S., Yoshida N., Gao L., Navarro J., Thacker R., et al., 2005, *Nature*, 435, 629
- Tegmark M., Blanton M. R., Strauss M. A., Hoyle F., Schlegel D., Scoccimarro R., Vogeley M. S., Weinberg D. H., et al., 2004a, *ApJ*, 606, 702
- Tegmark M., Blanton M. R., Strauss M. A., Hoyle F., Schlegel D., Scoccimarro R., Vogeley M. S., Weinberg D. H., et al., 2004b, *ApJ*, 606, 702
- Tikhonov A. V., Gottlöber S., Yepes G., Hoffman Y., 2009, *MNRAS*, 399, 1611
- van de Weygaert R., Bertschinger E., 1996, *MNRAS*, 281, 84
- Wang H., Mo H. J., Yang X., van den Bosch F. C., 2013, *ArXiv e-prints* 1301.1348
- White S. D. M., Rees M. J., 1978, *MNRAS*, 183, 341
- Yahil A., Strauss M. A., Davis M., Huchra J. P., 1991, *ApJ*, 372, 380
- Zaroubi S., Hoffman Y., Dekel A., 1999, *ApJ*, 520, 413
- Zavala J., Jing Y. P., Faltenbacher A., Yepes G., Hoffman Y., Gottlöber S., Catinella B., 2009, *ApJ*, 700, 1779
- Zel'dovich Y. B., 1970, *Astr.Astrophys.*, 5, 84